Surface & Coatings Technology 251 (2014) 1–6

Contents lists available at ScienceDirect

Surface & Coatings Technology

journal homepage: www.elsevier.com/locate/surfcoat

# Structural and nanoindentation studies of epitaxial titanium oxynitride (001) films grown on MgO(001) substrate

Hien Do [a,*], Van-Truong Dai [b], Jr-Sheng Tian [a], Tzu-Chun Yen [a], Li Chang [a]

[a] Department of Materials Science and Engineering, National Chiao Tung University, Hsinchu 300, Taiwan, ROC
[b] Department of Electronics Engineering, National Chiao Tung University, Hsinchu 300, Taiwan, ROC

ARTICLE INFO

*Article history:*
Received 11 December 2013
Accepted in revised form 27 March 2014
Available online 4 April 2014

*Keywords:*
Epitaxial titanium oxynitride
Nanoindentation
Mechanical properties

ABSTRACT

We investigate the effect of chemical composition and residual stress on the mechanical properties of high-quality epitaxial $TiN_xO_y$ films deposited on MgO(001) substrates by using nanoindentation. The lattice parameters and residual strain/stress of $TiN_xO_y$ films decrease as oxygen concentration increases. Hardness and Young's modulus determined by nanoindentation are about 17–26 GPa and 355–430 GPa, respectively, which vary with chemical composition and residual stress.



## 1. Introduction

Titanium belongs to the group IV B metals and it presents the binary solid solution of "TiN–TiO" or titanium oxynitride. This solid solution, named $TiN_xO_y$, has the same NaCl structure with that of TiN and TiO. Recently, titanium oxynitride ($TiN_xO_y$) has been extensively studied because it combines many remarkable properties of both titanium nitride (hardness, wear resistance) and titanium oxide (chemical stability, optical properties) [1]. It is of great interest that the optical, electrical, and mechanical properties of titanium oxynitride can be tailored between metallic nitride (TiN) and the corresponding ionic oxide (TiO) by varying the N/O ratio [2,3]. Therefore, titanium oxynitride can be considered as strong candidates in a wide range of applications such as decorative and wear-resistant coating [2,3], transparent IR window electrodes [2], solar collector devices [2,4], electrical switchable windows [5], photocatalysis [6], biomaterials [7,8], and memory devices [9]. Most of studies have focused on the chemical composition and the optical and electrical properties of polycrystalline titanium oxynitride [2,3,10–12]. However, there have been few reports on the mechanical properties of $TiN_xO_y$ films, especially epitaxial $TiN_xO_y$ films. This is due to the difficulty in deposition of epitaxial $TiN_xO_y$ and the fact that mechanical properties of $TiN_xO_y$ depend on not only chemical composition but also microstructure, whereas microstructure of polycrystalline $TiN_xO_y$ films varies widely and is often uncharacterized.

In our previous report, high-quality epitaxial (001) titanium oxynitride films with different composition have been successfully grown on MgO substrates by pulsed laser deposition (PLD) [13]. In this work, the mechanical properties of the deposited titanium oxynitride films are characterized by using nanoindentation. We also investigate the effect of chemical composition and residual stress on the mechanical properties of titanium oxynitride films.

Nanoindentation has been the most commonly used technique in characterizing the mechanical properties of materials on nanoscale. Based on the data obtained from nanoindentation testing, the method given by Oliver and Pharr [14] has been widely used to determine the approximate hardness and modulus of thin films. This method, however, does not take into account the substrate effect, and therefore it cannot be applied for the film/substrate systems with a significant elastic mismatch between films and substrates, especially at a wide range of indentation depths. A number of different methods have been developed in an attempt to model the substrate effect [15–18]. In this article, to exclude the substrate effect and obtain accurate hardness and modulus of thin $TiN_xO_y$ films on MgO substrate as there exists a large elastic mismatch between film and substrate, we applied the model developed by Li and Vlassak [18]. In this model, a data analysis procedure based on Yu's elastic solution was used to derive the projected-contact area of an elasto-plastic indentation. From the projected-contact area, the hardness and elastic modulus of the film/substrate systems with a large elastic mismatch can be extracted even at high indentation depths.

## 2. Experimental

Epitaxial $TiN_xO_y$ films were grown on 50-mm MgO substrates (thickness of 0.275 mm) by PLD using a KrF ($\lambda = 248$ nm) laser. MgO has been chosen as substrate for the deposition of high-quality $TiN_xO_y$ films because MgO also has NaCl structure and its lattice constant is very close to those of TiN and TiO. All the films were deposited at substrate temperature of 700 °C. To obtain $TiN_xO_y$ films with different

* Corresponding author. Tel.: +886 3 5731615; fax: +886 3 5724727.
*E-mail address:* dohienvl@gmail.com (H. Do).

http://dx.doi.org/10.1016/j.surfcoat.2014.03.058
0257-8972/

**Table 1**
Chemical composition, thickness, in-plane $a$, out-of plane $c$, and relaxed $a_o$ lattice parameters, FWHM of (002) $TiN_xO_y$, in-plane residual strain $\varepsilon_{||}$ and stress $\sigma_{||}$, and critical thickness $h_c$ of $TiN_xO_y$ films.

| Sample | 1 | 2 | 3 | 4 |
|---|---|---|---|---|
| Chemical composition | $TiN_{1.11}O_{0.10}$ | $TiN_{0.97}O_{0.23}$ | $TiN_{0.81}O_{0.38}$ | $TiN_{0.63}O_{0.55}$ |
| Thickness | 41 nm | 76 nm | 120 nm | 110 nm |
| FWHM of (002) TiNO | 62 | 58 | 60 | 61 |
| $a$ (Å) | 4.2124 | 4.2116 | 4.2121 | 4.2112 |
| $c$ (Å) | 4.2577 | 4.2541 | 4.2412 | 4.2231 |
| $a_o$ (Å) | 4.2414 | 4.2388 | 4.2307 | 4.2188 |
| $\varepsilon_{||}$ (%) | −0.69 | −0.65 | −0.44 | −0.18 |
| $\sigma_{||}$ (GPa) | −3.77 | −3.53 | −2.43 | −0.99 |
| $h_c$ (nm) | 9.6 | 10.4 | 17 | 49 |

chemical composition, a 50-mm titanium oxynitride target (composition of $TiNO_{0.064}$) was used, and the deposition process was carried out under base pressure of $133 \times 10^{-6}$ Pa and in the nitrogen gas ambient varies from $133 \times 10^{-3}$ to $133 \times 10^{-5}$ Pa. The detailed deposition procedure was described elsewhere [13]. X-ray photoelectron spectroscopy (XPS) (ULVAC-PHI, PHI Quantera SXM) with monochromatic Al Kα radiation source was used to determine the film composition. Prior to the XPS analysis, the film surface was cleaned by Ar ion sputtering for 60 s. The XPS quantification analysis was then carried out by using the peak area corrected with the relative sensitivity factors from manufacture's program and database. A Bede D1 high-resolution X-ray diffractometer, equipped with a two-bounce Si 220 channel-cut collimator crystal, a dual channel Si 220 analyzer crystal, and $CuK\alpha_1$ radiation ($\lambda = 0.15406$ nm), was used to investigate the crystallinity and to calculate the residual stress tensors of the films.

In our experiments, the mechanical properties of $TiN_xO_y$ films (sample area of $1 \times 1$ cm$^2$) were characterized using a MTS Nanoindenter XP system with a diamond Berkovich tip with an apex angle of 65.30° and a tip radius of about 20 nm. The continuous-stiffness-measurement (CSM) mode was used with a harmonic force at 45 Hz imposed on the increasing load. The Berkovich tip shape (area function) was calibrated using a fused silica specimen to ensure the accuracy of the indentation measurements. The indentation procedure consisted of five steps: loading to the specified indentation depth, holding the indenter at the peak load for 10 s, unloading 5% of the peak load, holding the indenter at this point for 60 s for thermal drift correction, and unloading completely. Five indentations were performed for each deposited film and MgO substrate, and the average results of the group are presented here. The indentation data of all $TiN_xO_y$/MgO samples were then analyzed using the procedure given by Li and Vlassak as described in detail in Ref. [18], while the indentation data of MgO substrates were analyzed using the method of Oliver and Pharr [14]. All the analysis procedure was carried out by using mathematical software Matlab. Li and Vlassak [18] have also shown that Poisson's ratio of the film has a minor effect on nanoindentation results. In the analysis procedure, therefore, we used the Poisson's ratio of TiN ($\nu_{TiN} = 0.22$) for all as-deposited $TiN_xO_y$ films. The results are also compared with the ones that are calculated by the commonly used method of Oliver and Pharr [14].

## 3. Results and discussion

Chemical composition of as-deposited $TiN_xO_y$ films was determined by XPS and listed in Table 1. As described elsewhere [13], the XPS spectra of Ti-2p, O-1 s, and N-1 s examined in high-resolution mode revealed that the $TiN_xO_y$ films consist of three components of titanium nitride, titanium oxynitride, and titanium dioxide. The X-ray 2θ–θ (Fig. 1) and ϕ-scan combined with transmission electron microscopy analysis have shown that all the deposited films are epitaxial $TiN_xO_y(001)$ with a cube-on-cube relationship to the MgO substrate: $TiN_xO_y(001)$//MgO(001) and $TiN_xO_y[100]$//MgO[100] [13]. In the X-ray 2θ–θ scan, $TiN_xO_y(002)$ peak position ranges from 42.598° ($TiN_{1.1}O_{0.10}$) to 42.852° ($TiN_{0.63}O_{0.55}$) due to corresponding changes in film composition and residual strain. The finite-thickness interference fringes in high-resolution X-ray diffraction (XRD) 2θ–θ scans (Fig. 1) indicate that $TiN_xO_y$ surfaces and $TiN_xO_y$/MgO interfaces are smooth. The full width at half maximum (FWHM) of $TiN_xO_y(002)$ determined by X-ray rocking curve scans are about 58–62 arcsec (shown in Table 1). The thickness of the $TiN_xO_y$ films can be determined from the X-ray reflectivity curves and the results are listed in Table 1. High-resolution XRD reciprocal space maps (RSM) of asymmetric (113) MgO and (113) $TiN_xO_y$ reflections were also acquired (Fig. 2). The RSM images show that (113) $TiN_xO_y$ reflections of all the films are almost vertically aligned with (113) MgO. This indicates that all the deposited $TiN_xO_y$ films are under full compressive strain. From the RSM images, the out-of-plane $c$, in-plane $a$, and relaxed lattice parameters $a_o$, and in-plane residual strain $\varepsilon_{||}$ and stress $\sigma_{||}$ can be determined and are presented in Table 1. The results reveal that the lattice parameters of $TiN_xO_y$ films decrease with increased oxygen content due to the smaller radius of oxygen anion compared with that of nitrogen and the decrease in the electrostatic repulsion between the anions around Ti vacancies when N atoms are replaced by O atoms [13]. Theoretical critical thickness $h_c$ (Table 1) of $TiN_xO_y$ films is calculated by using Matthews and Blakeslee model [19]. As shown in Fig. 2 and Table 1, all the deposited films are under full compressive strain due to thermal mismatch and lattice mismatch between $TiN_xO_y$ and MgO. Stress is not relaxed in all the films, especially in the $TiN_xO_y$ films with low oxygen content, for which the thickness is much larger than the predicted critical thickness $h_c$. This could be explained from the viewpoint of the critical shear stress for the dislocation nucleation. Indeed, an experimental investigation has shown that the critical shear stress $\tau_{crit}$ for the dislocation nucleation in a single crystal TiN(001) [20] is about $G/50$ ($G$ is the shear modulus for TiN). In the case of $TiN_xO_y$ films with low oxygen content, we can also assume $\tau_{crit} \sim G/50$. To evaluate the possibility for dislocation nucleation in the $TiN_xO_y$ films, we calculated the complete residual stress tensors of the films by using the multiple asymmetric X-ray diffraction method [21]. From the residual stress tensors, the principal stresses $\sigma_1$, $\sigma_2$, and $\sigma_3$ [22] and maximum shear stresses $\tau_{max}$ acting on the {110} planes

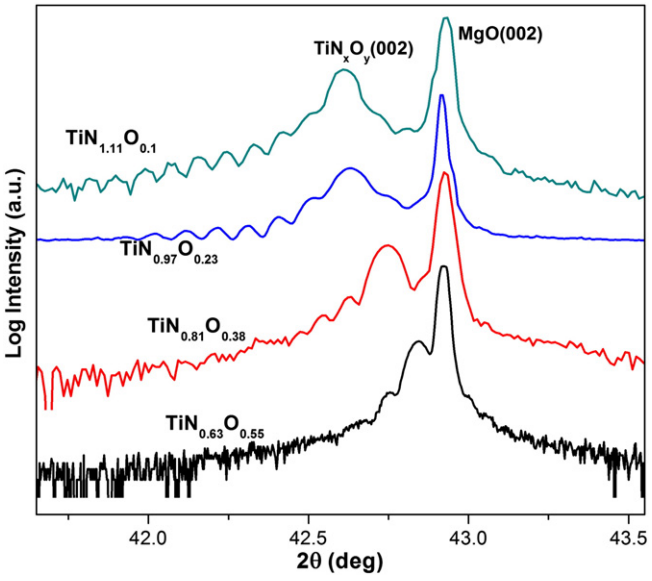


**Fig. 1.** High-resolution XRD 2θ–θ scans for epitaxial $TiN_xO_y$ films with different chemical composition deposited on MgO substrates.

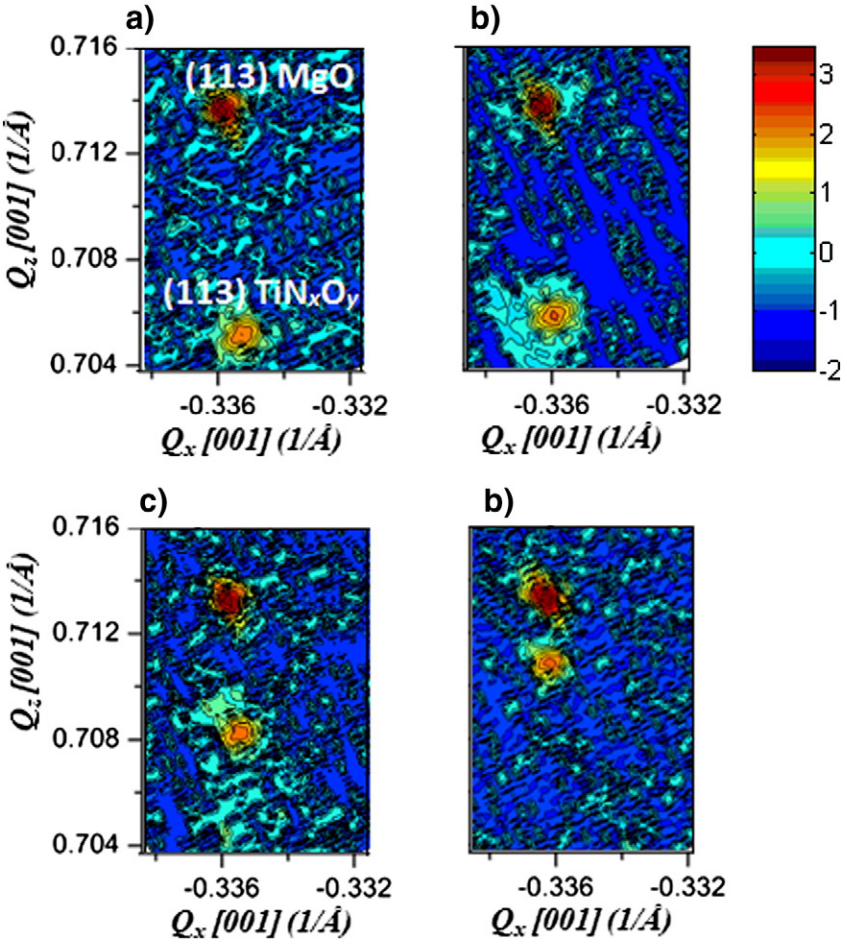


**Fig. 2.** Reciprocal space maps of the asymmetric (113) MgO and (113) $TiN_xO_y$ reflections with different composition of a) $TiN_{1.1}O_{0.10}$, b) $TiN_{0.97}O_{0.23}$, c) $TiN_{0.81}O_{0.38}$ and d) $TiN_{0.63}O_{0.55}$.

[23] can be calculated and presented in Table 2. The values of $\tau_{crit} \sim G/50$ are also listed in Table 2 for comparison. The results clearly show that the maximum shear stresses in the $TiN_xO_y$ films are about 2–6 times lower than critical shear stress for dislocation nucleation. Therefore, no stress relaxation caused by dislocations could be observed in the $TiN_xO_y$ films. Similar behavior without relaxation can be also observed in epitaxial $TiN_x$ ($0.67 \leq x \leq 1$) films [24], in which the film thickness is much larger than the critical thickness (more than 10 times).

Nanoindentation results of all the $TiN_xO_y$ films and MgO are summarized in Table 3. The hardness and Young's modulus of MgO obtained using Oliver–Pharr method are in good agreement with the reported values in the literatures [25,26]. The results show that the hardnesses and Young's moduli of the deposited $TiN_xO_y$ films are in range of 17–26 GPa and 355–450 GPa, respectively. The $TiN_xO_y$ film with small oxygen concentration shows that the Young's modulus is closed to the reported value of stoichiometric single-crystal TiN(001) with $E \sim 445 \pm 38$ GPa, while the hardness value is larger than that of stoichiometric single-crystal TiN(001) with $H \sim 20 \pm 0.8$ GPa [27]. Fig. 3 illustrates the Young's modulus of the $TiN_xO_y$ films obtained using the Li–Vlassak approach in comparison with the values obtained from the Oliver–Pharr method as a function of indentation depth divided by film thickness $h/t$. As expected, the obtained Oliver–Pharr moduli are noisy and fall sharply at small indentation depths and quickly approach the substrate modulus with increasing $h/t$ due to the substrate effect that not excluded from the calculated results. In contrast, the film moduli obtained from the Li–Vlassak method, in which the substrate effect caused by film-substrate elastic mismatch has been taken into account, are constant throughout a wide range of indentation depths. Fig. 4 shows the hardness of each $TiN_xO_y$ film as a function of indentation depth calculated using both the Li–Vlassak and Oliver–Pharr methods, together with the hardness value of MgO substrate. Both methods show that each $TiN_xO_y$ hardness curve rises from zero value

**Table 2**
The principal stress $\sigma_1$, $\sigma_2$, and $\sigma_3$, maximum shear stress $\tau_{max}$, and the critical shear stress $\tau_{crit}$ [20] of $TiN_xO_y$ films.

| | $TiN_{1.11}O_{0.10}$ | $TiN_{0.97}O_{0.23}$ | $TiN_{0.81}O_{0.38}$ | $TiN_{0.63}O_{0.55}$ |
|---|---|---|---|---|
| $\sigma_1$ (GPa) | 0.0018 | 0.00052 | 0.00065 | 0.0035 |
| $\sigma_2$ (GPa) | −3.678 | −3.457 | −2.377 | −0.963 |
| $\sigma_3$ (GPa) | −3.854 | −3.612 | −2.776 | −1.02 |
| $\tau_{max}$ (GPa) | 1.93 | 1.81 | 1.39 | 0.51 |
| $\tau_{crit}$ (GPa) | 3.52 | 3.29 | 3.16 | 2.91 |

**Table 3**
The hardness and Young's modulus of $TiN_xO_y$ films calculated by using Li–Vlassak method [18].

| Sample | Poisson's ratio | $E$ (GPa) | $H$ (GPa) |
|---|---|---|---|
| MgO | 0.19 | 300 ± 3.2 | 10 ± 1 |
| $TiN_{1.11}O_{0.10}$ | 0.22 | 430 ± 5.7 | 26 ± 1.2 |
| $TiN_{0.97}O_{0.23}$ | 0.22 | 400 ± 7.3 | 23 ± 1.7 |
| $TiN_{0.81}O_{0.38}$ | 0.22 | 385 ± 5.2 | 21 ± 1.3 |
| $TiN_{0.63}O_{0.55}$ | 0.22 | 355 ± 4.6 | 17 ± 1.2 |

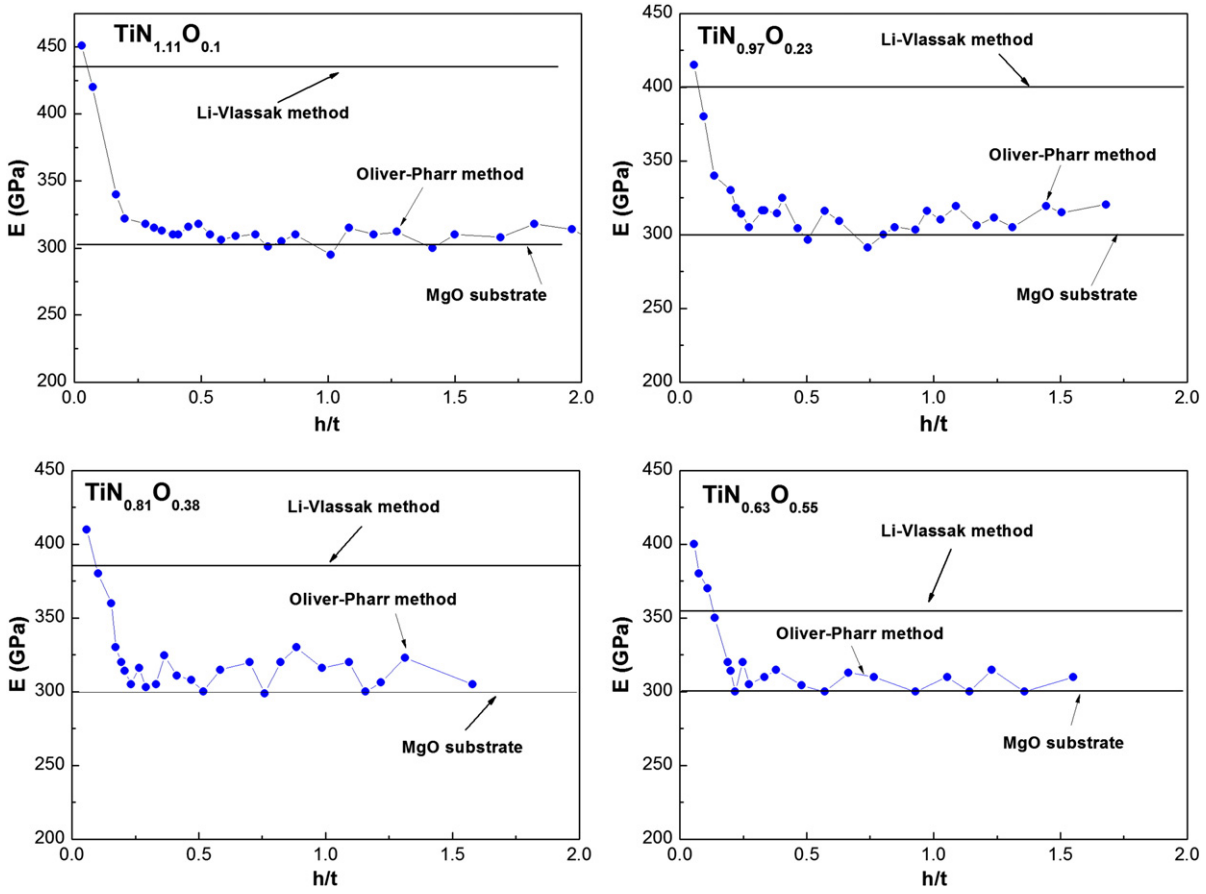


**Fig. 3.** The Young's modulus of $TiN_xO_y$ films as a function of $h/t$ (indentation depth/film thickness) obtained by using Li–Vlassak method, together with the Young's modulus of MgO substrate. The results obtained using Oliver–Pharr method are presented for comparison.

at shallow indentation depths and reaches a maximum value as indentation depth increases. It is noticed that the hardness curves drop off and reach the substrate hardness value rapidly when the indenter approaches film/substrate interface due to the extensive plastic deformation in the soft substrate. However, the maximum hardness values obtained from Oliver–Pharr analysis are significantly lower compared with those from of Li–Vlassak method due to the effect of the soft substrate. This indicates that the effect of film-substrate elastic mismatch is significantly excluded from the results obtained by Li–Vlassak analysis.

It is also seen that the mechanical property measurements of the $TiN_xO_y$ films are consistent with both chemical composition and residual stress. Both $H$ and $E$ of the $TiN_xO_y$ films decrease with increasing oxygen content and increase with increasing nitrogen content. The maximum values of $H$ and $E$ were found for the $TiN_xO_y$ film with the highest nitrogen content that correspond with the highest residual stress value. The $TiN_xO_y$ film with the highest oxygen content, and the lowest residual stress as consequence, shows the minimum values of $H$ and $E$. Fig. 5 presents the linear increasing of $H$ and $E$ with residual compressive stress. The dependence of the mechanical properties of $TiN_xO_y$ on oxygen and nitrogen content can be explained by the changes in covalent and ionic contribution to the bond in the $TiN_xO_y$ compound. Indeed, it has been shown in Ref. [25] that the increase of oxygen substituting for nitrogen leads to a decrease in covalent contribution to the bond. As a consequence, the bond has a higher ionic character that causes bond strength to decrease (the bond lengths can be considered as constants due to the reason that the bond length decreases by less than 0.5% when $x$ decreases from 1.1 to 0.63 and $y$ increases from 0.1 to 0.55). Similarly, the increase of nitrogen content leads to an increase in covalent character of the bond, and thereby bond strength, increases. Hence, hardness and elastic modulus increases as the amount of nitrogen increases, and decreases as the amount of oxygen increases. Similar behavior of $H$ and $E$ with chemical composition has also been reported for polycrystalline, textured, and bulk $TiN_xO_y$ [2,12,28,29]. Therefore, the increase of oxygen can be considered as a softening factor on the $TiN_xO_y$ films.

As seen in the XRD data above, the change in stoichiometry of the films causes the change in the residual compressive stress. From the viewpoint of atomic bonding force to interatomic spacing, the difference in residual compressive stress could also have an influence on the mechanical property measurements of the films [30–32]. Indeed, it is known that atoms locate at a balanced interatomic separation $r_o$, and the spacing changes under a force. If the interatomic separation exceeds the maximum value $r_{max}$ under an applied force over the maximum atomic bonding force $F_{max}$, atomic bonds will be broken, and deformation will initiate. The residual compressive stress will make interatomic spacing compressed, and a larger applied force may be needed to break bonds. Therefore, an increase in $H$ and $E$ can be expected when residual compressive stress increases. Similar variations of $H$ and $E$ with residual compressive stress have also been reported for polycrystalline $TiN_xO_y$ film [29] and other materials [30,31,33,34].

## 4. Conclusions

Microstructure and mechanical properties of high-quality epitaxial $TiN_xO_y$ films with different composition ($0.63 < x < 1.11$, $0.1 < y < 0.55$)

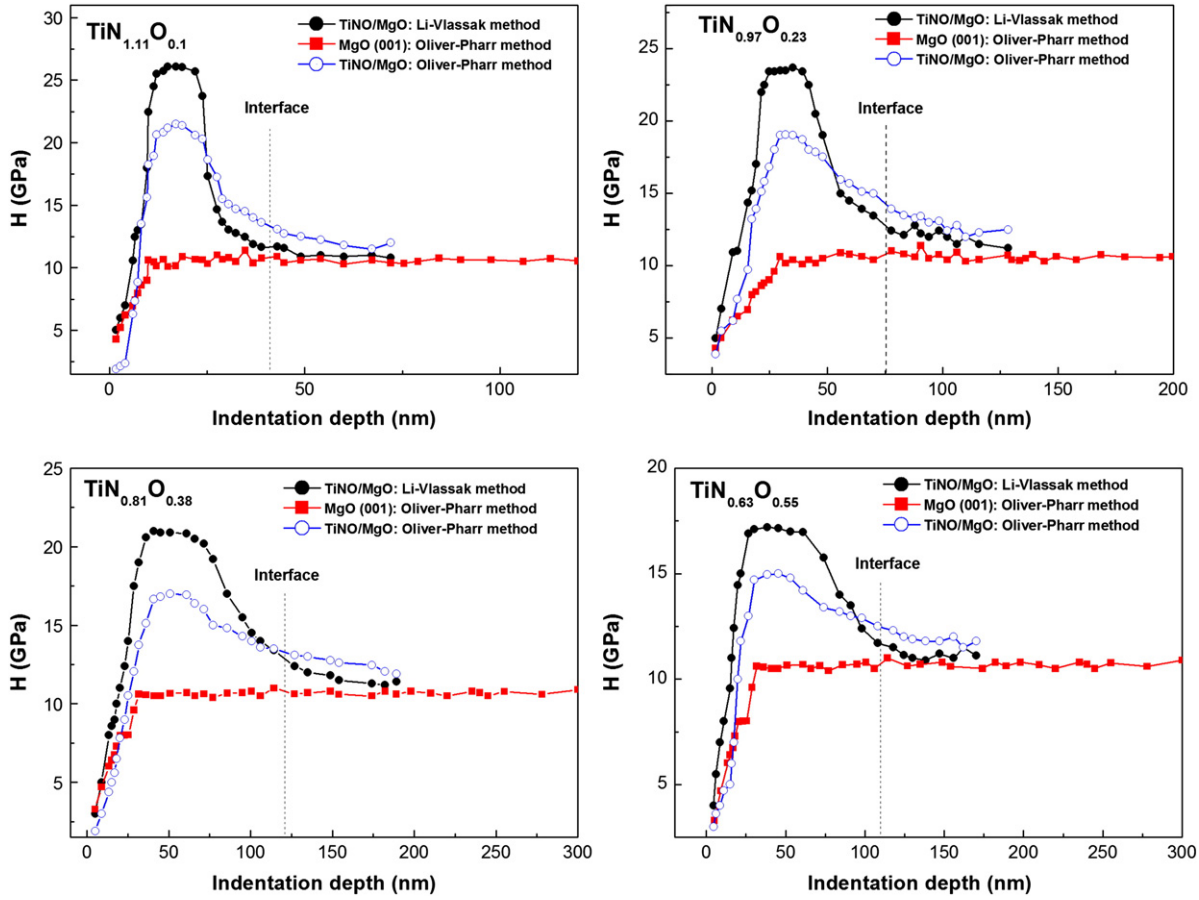


**Fig. 4.** The hardness of $TiN_xO_y$ films as a function of indentation depth calculated by using both Li–Vlassak and Oliver–Pharr methods. The hardness value of MgO substrate is also included.

deposited on MgO by PLD method have been characterized. The lattice parameter and residual compressive stress are shown to decrease with *x*. The Li–Vlassak method for analysis of nanoindentation of hard $TiN_xO_y$ film on soft MgO substrate is used to provide the values for hardness and Young's modulus of about 17–26 GPa and 355–430 GPa, respectively. Both *H* and *E* are found to decrease with increasing of oxygen and decreasing of residual stress, and increase with increasing of nitrogen content and residual stress.

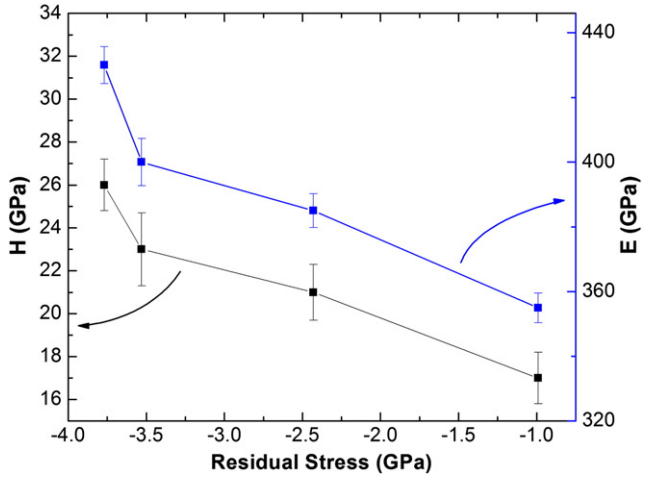


**Fig. 5.** Evolution of the hardness and Young's modulus of $TiN_xO_y$ films with residual compressive stress.

## Conflict of interest

There is no conflict of interest.

## Acknowledgments

The work was supported by the National Science Council, Taiwan, R.O.C. under Contract No. NSC 101-2221-E-009-050-MY3.

## References

[1] J.M. Chappe, N. Martin, G. Terwagne, J. Lintymer, J. Gavoille, J. Takadoum, Thin Solid Films 440 (2003) 66–73.
[2] M. Braic, M. Balaceanu, A. Vladescu, A. Kiss, V. Braic, G. Epurescu, G. Dinescu, A. Moldovan, R. Birjega, M. Dinescu, Appl. Surf. Sci. 253 (2007) 8210–8214.
[3] F. Vaz, P. Cerqueira, L. Rebouta, S.M.C. Nascimento, E. Alves, P. Goudeau, J.E. Riviere, Surf. Coat. Technol. 174 (2003) 197–203.
[4] M. Lazarov, P. Raths, H. Metzger, W. Spirkl, J. Appl. Phys. 77 (1995) 2133–2137.
[5] Y. Saito, M. Hirata, H. Tada, M. Hyodo, Appl. Phys. Lett. 63 (1993) 1319–1321.
[6] R. Asahi, T. Morikawa, T. Ohwaki, K. Aoki, Y. Taga, Science 293 (2001) 269–271.
[7] Y.X. Leng, P. Yang, J.Y. Chen, H. Sun, J. Wang, G.J. Wang, N. Huang, X.B. Tian, P.K. Chu, Surf. Coat. Technol. 138 (2001) 296–300.
[8] R.J. Koerner, L.A. Butterworth, I.V. Mayer, R. Dasbach, H.J. Busscher, Biomaterials 23 (2002) 2835–2840.
[9] D.-H. Kang, D.-H. Ahn, M.-H. Kwon, H.-S. Kwon, K.-B. Kim, K.S. Lee, B.-k. Cheong, Jpn. J. Appl. Phys. 43 (2004) 5243–5244.
[10] X.G. Yang, C. Li, B.J. Yang, W. Wang, Y.T. Qian, Chem. Phys. Lett. 383 (2004) 502–506.
[11] E. Vogelzang, J. Sjollema, H.J. Boer, J.T.M. Dehosson, J. Appl. Phys. 61 (1987) 4606–4611.
[12] J.M. Chappe, N. Martin, J. Lintymer, F. Sthal, G. Terwagne, J. Takadoum, Appl. Surf. Sci. 253 (2007) 5312–5316.
[13] H. Do, Y.H. Wu, V.T. Dai, C.Y. Peng, T.C. Yen, L. Chang, Surf. Coat. Technol. 214 (2013) 91–96.
[14] W.C. Oliver, G.M. Pharr, J. Mater. Res. 7 (1992) 1564–1583.
[15] R.B. King, Int. J. Solids Struct. 23 (1987) 1657–1664.
[16] R. Saha, W.D. Nix, Acta Mater. 50 (2002) 23–38.

[17] S.M. Han, R. Saha, W.D. Nix, Acta Mater. 54 (2006) 1571–1581.
[18] H. Li, J.J. Vlassak, J. Mater. Res. 24 (2009) 1114–1126.
[19] J.W. Matthews, A.E. Blakeslee, J. Cryst. Growth 27 (1974).
[20] M. Oden, M. Ljungcrantz, L. Hultman, J. Mater. Res. 12 (1997) 2134–2142.
[21] M. Liu, L.C. Zhang, A. Brawley, P. Atanackovic, S. Duvall, Adv. Mater. Proc. I 443 (2010) 742–747.
[22] L.C. Zhang, Solid Mechanics for Engineers, Palgrave Mcmillan, 2001.
[23] A. Kelly, G.W. Groves, P. Kidd, Crystallography and Crystal Defects, Wiley, 2000.
[24] C.S. Shin, D. Gall, N. Hellgren, J. Patscheider, I. Petrov, J.E. Greene, J. Appl. Phys. 93 (2003) 6025–6028.
[25] D. Caceres, I. Vergara, R. Gonzalez, Y. Chen, E. Alves, Nucl. Inst. Methods Phys. Res. B 191 (2002) 154–157.
[26] K. Kurosaki, D. Setoyama, J.J. Matsunaga, S. Yamanaka, J. Alloys Compd. 386 (2005) 261–264.
[27] H. Ljungcrantz, M. Oden, L. Hultman, J.E. Greene, J.E. Sundgren, J. Appl. Phys. 80 (1996) 6725–6733.
[28] J. Graciani, S. Hamad, J.F. Sanz, Phys. Rev. B 80 (2009) 184112–184122.
[29] F. Vaz, P. Cerqueira, L. Rebouta, S.M.C. Nascimento, E. Alves, P. Goudeau, J.R. Riviere, K. Pischow, J. de Rijk, Thin Solid Films 447 (2004) 449–454.
[30] Y.C. Huang, S.Y. Chang, C.H. Chang, Thin Solid Films 517 (2009) 4857–4861.
[31] A. Mallik, B.C. Ray, Surf. Eng. 27 (2011) 551–556.
[32] T.H. Courtney, Mechanical Behavior of Materials, McGrill-Hill, New York USA, 1990.
[33] L. Karlsson, L. Hultman, J.E. Sundgren, Thin Solid Films 371 (2000) 167–177.
[34] A. Mani, P. Aubert, F. Mercier, H. Khodja, C. Berthier, P. Houdy, Surf. Coat. Technol. 194 (2005) 190–195.